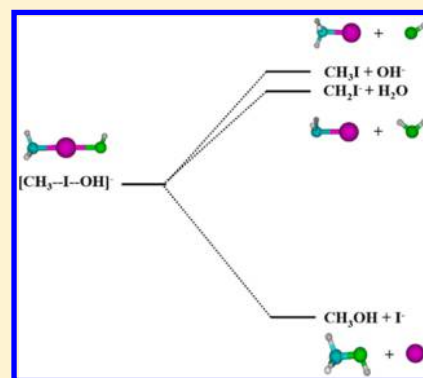


# Direct Dynamics Simulation of Dissociation of the $[\text{CH}_3\text{--I--OH}]^-$ Ion–Molecule Complex

Jing Xie,<sup>†</sup> Miranda McClellan,<sup>†,‡</sup> Rui Sun,<sup>†</sup> Swapnil C. Kohale,<sup>†</sup> Niranjan Govind,<sup>§</sup> and William L. Hase<sup>\*,†</sup><sup>†</sup>Department of Chemistry and Biochemistry, Texas Tech University, Lubbock, Texas 79409, United States<sup>‡</sup>School for the Talented and Gifted, 1201 East Eighth Street, Suite 302, Dallas, Texas 75203, United States<sup>§</sup>Environmental Molecular Sciences Laboratory, Pacific Northwest National Laboratory, Richland, Washington 99352, United States

## Supporting Information

**ABSTRACT:** Direct dynamics simulations were used to study dissociation of the  $[\text{CH}_3\text{--I--OH}]^-$  complex ion, which was observed in a previous study of the  $\text{OH}^- + \text{CH}_3\text{I}$  gas phase reaction (*J. Phys. Chem. A* **2013**, *117*, 7162). Restricted B97-1 simulations were performed to study dissociation at 65, 75, and 100 kcal/mol and the  $[\text{CH}_3\text{--I--OH}]^-$  ion dissociated exponentially, in accord with RRKM theory. For these energies the major dissociation products are  $\text{CH}_3\text{I} + \text{OH}^-$ ,  $\text{CH}_2\text{I}^- + \text{H}_2\text{O}$ , and  $\text{CH}_3\text{OH} + \text{I}^-$ . Unrestricted B97-1 and restricted and unrestricted CAM-B3LYP simulations were also performed at 100 kcal/mol to compare with the restricted B97-1 results. The  $\{\text{CH}_3\text{I} + \text{OH}^-\}:\{\text{CH}_2\text{I}^- + \text{H}_2\text{O}\}:\{\text{CH}_3\text{OH} + \text{I}^-\}$  product ratio is 0.72:0.15:0.13, 0.81:0.05:0.14, 0.71:0.19:0.10, and 0.83:0.13:0.04 for the restricted B97-1, unrestricted B97-1, restricted CAM-B3LYP, and unrestricted CAM-B3LYP simulations, respectively. Other product channels found are  $\text{CH}_2 + \text{I}^- + \text{H}_2\text{O}$ ,  $\text{CH}_2 + \text{I}^-(\text{H}_2\text{O})$ ,  $\text{CH}_4 + \text{IO}^-$ ,  $\text{CH}_3^- + \text{IOH}$ , and  $\text{CH}_3 + \text{IOH}^-$ . The  $\text{CH}_3^- + \text{IOH}$  singlet products are only given by the restricted B97-1 simulation and the lower energy  $\text{CH}_3 + \text{IOH}^-$  doublet products are only formed by the unrestricted B97-1 simulation. Also studied were the direct and indirect atomic-level mechanisms for forming  $\text{CH}_3\text{I} + \text{OH}^-$ ,  $\text{CH}_2\text{I}^- + \text{H}_2\text{O}$ , and  $\text{CH}_3\text{OH} + \text{I}^-$ . The majority of  $\text{CH}_3\text{I} + \text{OH}^-$  were formed through a direct mechanism. For both  $\text{CH}_2\text{I}^- + \text{H}_2\text{O}$  and  $\text{CH}_3\text{OH} + \text{I}^-$ , the direct mechanism is overall more important than the indirect mechanisms, with the roundabout like mechanism the most important indirect mechanism at high excitation energies. Mechanism comparisons between the B97-1 and CAM-B3LYP simulations showed that formation of the  $\text{CH}_3\text{OH--I}^-$  complex is favored for the B97-1 simulations, whereas formation of the  $\text{HO}^- \text{---} \text{HCH}_2\text{I}$  complex is favored for the CAM-B3LYP simulations. The unrestricted simulations give a higher percentage of indirect mechanisms than the restricted simulations. The possible role of the self-interaction error in the simulations is also discussed. The work presented here gives a detailed picture of the  $[\text{CH}_3\text{--I--OH}]^-$  dissociation dynamics and is very important for unraveling the role of  $[\text{CH}_3\text{--I--OH}]^-$  in the dynamics of the  $\text{OH}^-(\text{H}_2\text{O})_{n=1,2} + \text{CH}_3\text{I}$  reactions.



## I. INTRODUCTION

In previous work the dynamics of the  $\text{OH}^- + \text{CH}_3\text{I}$  ion–molecule reaction was studied by both experiments<sup>1,2</sup> and simulations.<sup>3–5</sup> The reaction has multiple products, with the dominant products those for the  $\text{S}_{\text{N}}2$  and proton-transfer pathways,  $\text{CH}_3\text{OH} + \text{I}^-$  and  $\text{CH}_2\text{I}^- + \text{H}_2\text{O}$ , respectively. Less important products are  $\text{IOH}^- + \text{CH}_3$  and  $\text{CH}_2 + \text{I}^- + \text{H}_2\text{O}$ . A both interesting and important reaction intermediate observed in the simulations is  $[\text{CH}_3\text{--I--OH}]^-$ . Similar intermediates  $[\text{CF}_3\text{--X--F}]^-$  ( $\text{X} = \text{Br}, \text{I}$ ) and  $[\text{CH}_3\text{--Br--Cl}]^-$  were proposed by Viggiano and co-workers in their studies<sup>6–8</sup> of ion–molecule reactions.

$[\text{CH}_3\text{--I--OH}]^-$ , formed by  $\text{CH}_3\text{I} + \text{OH}^-$  association, has sufficient energy to dissociate and is not observed in low pressure experiments, where collisional stabilization is unimportant. However, this complex is observed in microsolvation experiments for  $\text{OH}^-(\text{H}_2\text{O})_{n=1,2} + \text{CH}_3\text{I}$ , where  $[\text{CH}_3\text{--I--OH}]^-$  is stabilized by the transfer of energy to the  $\text{H}_2\text{O}$  molecule(s).

As shown in Figures 1 and 2,  $[\text{CH}_3\text{--I--OH}]^-$  has an interesting potential energy curve. It may isomerize to the hydrogen-bonded complex  $\text{HO}^- \text{---} \text{HCH}_2\text{I}$ , from which it can form the  $\text{S}_{\text{N}}2$  products  $\text{CH}_3\text{OH} + \text{I}^-$  or the proton-transfer complex  $\text{H}_2\text{O} \text{---} \text{CH}_2\text{I}^-$ . The latter can dissociate to  $\text{H}_2\text{O} + \text{CH}_2\text{I}^-$ . The  $[\text{CH}_3\text{--I--OH}]^-$  complex may also dissociate to  $\text{CH}_3 + \text{IOH}^-$ ,  $\text{CH}_2 + \text{I}^-(\text{H}_2\text{O})$ , and  $\text{CH}_2 + \text{I}^- + \text{H}_2\text{O}$ . With harmonic zero point energies (ZPEs) included, the respective barriers for forming the products  $\text{CH}_3\text{OH} + \text{I}^-$ ,  $\text{H}_2\text{O} + \text{CH}_2\text{I}^-$ ,  $\text{CH}_3 + \text{IOH}^-$ ,  $\text{I}^-(\text{H}_2\text{O}) + \text{CH}_2$ , and  $\text{CH}_2 + \text{I}^- + \text{H}_2\text{O}$  are 24.0, 24.0, 37.2, 44.3, and 54.2 kcal/mol. The dissociation barrier, with ZPE included, for returning to the  $\text{OH}^- + \text{CH}_3\text{I}$  reactants is 26.1 kcal/mol. The barriers for forming  $\text{CH}_3\text{OH} + \text{I}^-$ ,  $\text{CH}_2\text{I}^- + \text{H}_2\text{O}$ , and  $\text{CH}_3\text{I} + \text{OH}^-$  are the lowest and are similar, and

Received: November 29, 2014

Revised: January 8, 2015

Published: January 9, 2015

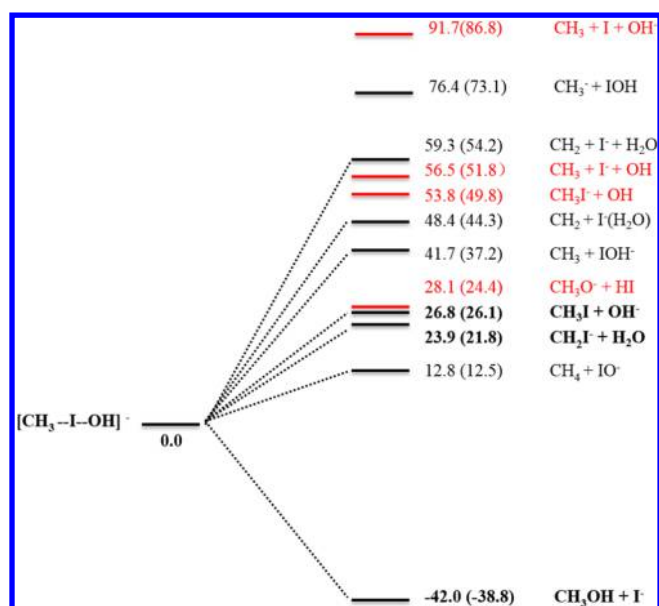


**Figure 1.** Potential energy profile for the dissociation of the  $[\text{CH}_3\text{--I--OH}]^-$  complex to different products. Energies (kcal/mol) are given by the B97-1/ECP/d method. The values without zero point energy are in normal text, and the zero point energy corrected energies are in parentheses. The products in red were not observed in the simulations.

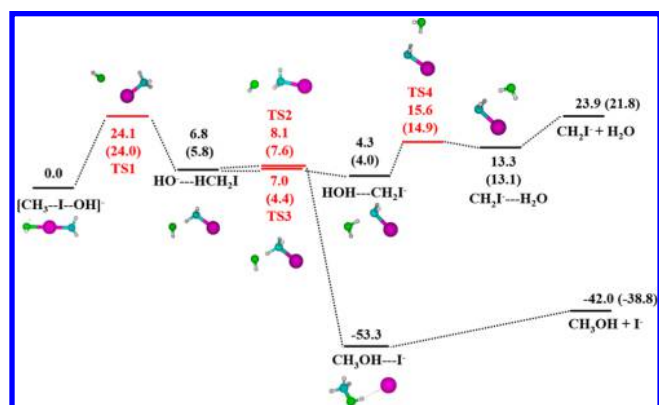


**Figure 2.** Schematic potential profiles for  $[\text{CH}_3\text{--I--OH}]^-$  dissociation to  $\text{CH}_3\text{OH} + \text{I}^-$  and  $\text{CH}_2\text{I}^- + \text{OH}^-$  on the  $S_N2$  and proton-transfer pathways. Energies (kcal/mol) are given by the B97-1/ECP/d method. The values without zero point energy are in normal text, and the zero point energy corrected energies are in parentheses.

the reaction pathways for forming these species are coupled as shown in Figure 2.

In the work reported here chemical dynamics simulations are performed to study the unimolecular dissociation of  $[\text{CH}_3\text{--I--OH}]^-$ . The complex is excited with a microcanonical ensemble of states at fixed total energies. The unimolecular rate constant and the branching between the product channels are calculated versus energy. The goal of this study is to determine the role of the  $[\text{CH}_3\text{--I--OH}]^-$  intermediate in the  $\text{OH}^- + \text{CH}_3\text{I}$  reaction, and understand its unimolecular dynamics to assist in interpreting chemical dynamics simulations of the  $\text{OH}^-(\text{H}_2\text{O})_{n=1,2} + \text{CH}_3\text{I}$  reactions.<sup>1,2</sup>

## II. COMPUTATIONAL METHODS

The NWChem<sup>9</sup> computer program was used to perform the electronic structure calculations. The direct dynamics simulations were performed with the VENUS/NWChem software package,<sup>10</sup> for which the VENUS chemical dynamics computer program<sup>11,12</sup> is interfaced with the NWChem<sup>9</sup> electronic structure computer program.

**A. Electronic Structure Calculations.** In previous work, DFT<sup>13</sup> with the B97-1<sup>14,15</sup> functional was used to characterize the potential energy surface (PES) for the  $\text{OH}^- + \text{CH}_3\text{I}$  reaction. Stationary points were identified and their structures, vibrational frequencies, and energies were determined. The basis set used for the calculations is called ECP/d,<sup>16</sup> for which Dunning and Woon's aug-cc-PVDZ basis set<sup>17,18</sup> is used for the H, C, and O atoms. For iodine, the Wadt and Hay effective core potential (ECP)<sup>19</sup> was used for the core electrons and a 3s, 3p basis set for the valence electrons, which was augmented by a d-polarization function with a 0.262 exponent, and s, p, and d diffuse functions with exponents of 0.034, 0.039, and 0.0873, respectively.<sup>20</sup> In previous studies, the restricted B97-1/ECP/d method was found to give overall reaction energetics<sup>2-4</sup> and dynamics<sup>3,4</sup> in good agreement with experiment for the  $\text{OH}^- + \text{CH}_3\text{I}$  reaction. Hence, this method was also used for the majority of the direct dynamics simulations reported here for  $[\text{CH}_3\text{--I--OH}]^-$  dissociation.

It was necessary to supplement the restricted B97-1/ECP/d direct dynamics with additional simulations. In careful analyses of the B97-1/ECP/d simulations it was found, for the  $[\text{CH}_3\text{--I--OH}]^-$  dissociation pathway to form  $\text{CH}_3\text{I} + \text{OH}^-$ , that  $\text{OH}^-$  was formed with a charge of approximately  $-0.8$  instead of the correct value of  $-1.0$ . Interestingly, such a problem was not present for the dissociation pathways  $\text{CH}_3\text{OH} + \text{I}^-$ ,  $\text{CH}_2\text{I}^- + \text{H}_2\text{O}$ ,  $\text{CH}_2 + \text{I}^-(\text{H}_2\text{O})$ , and  $\text{CH}_2 + \text{I}^- + \text{H}_2\text{O}$  identified in Figure 1. Nor was it present in our previous simulations of the  $\text{OH}^- + \text{CH}_3\text{I}$ , for which some of the trajectories scattered back to the reactants  $\text{OH}^- + \text{CH}_3\text{I}$ . Apparently, the previous trajectories formed  $\text{OH}^- + \text{CH}_3\text{I}$  appropriately because they did not form the  $[\text{CH}_3\text{--I--OH}]^-$  intermediate near its equilibrium

**Table 1.** Experimental and DFT<sup>a</sup> Reaction Enthalpies Relative to  $\text{CH}_3\text{I} + \text{OH}^-$

$\Delta H$	experiment		DFT	
	0 K	298 K	B97-1	CAM-B3LYP
$\text{CH}_3\text{OH} + \text{I}^-$	-66.44	$-66.91 \pm 0.26$	-64.87 (-68.80)	-66.71 (-70.60)
$\text{CH}_2\text{I}^- + \text{H}_2\text{O}$		$-3.12 \pm 1.82$	-4.23 (-2.88)	-1.39 (-0.07)
$\text{CH}_2 + \text{I}(\text{H}_2\text{O})^-$	$16.04 \pm 0.72$	$16.49 \pm 1.89$	18.20 (21.54)	17.32 (20.71)
$\text{CH}_3 + \text{IOH}^-$			11.10 (14.85)	5.98 (8.91)
$\text{CH}_2 + \text{I}^- + \text{H}_2\text{O}$	26.32	$26.77 \pm 1.17$	28.14 (32.44)	26.75 (31.25)
$[\text{CH}_3\text{--I--OH}]^-$			-26.08 (-26.82)	-22.44 (-23.39)

<sup>a</sup>Energies are in kcal/mol. For the DFT calculations, the energies in normal text are with zero point energy corrections, and values in parentheses are without zero point energy corrections. The experimental values may be found in ref 3.

geometry. Attempts were made to resolve the incorrect dissociation to  $\text{OH}^- + \text{CH}_3\text{I}$ , for the current study, by refining the simulations with a finer grid and tighter tolerance for the electronic density. However, this did not solve the problem and our understanding is that this could be from the self-interaction error in DFT,<sup>21–23</sup> an issue we plan to pursue in future studies.

Range-separated functionals like CAM-B3LYP<sup>24</sup> include an increasing fraction of Hartree–Fock exchange with increasing interelectronic separation, thus limiting the self-interaction error at large distances. This functional with parameters  $\alpha = 0.19$ ,  $\beta = 0.46$ , and  $\gamma = 0.33$  was used to ensure proper dynamics for  $[\text{CH}_3\text{--I--OH}]^- \rightarrow \text{CH}_3\text{I} + \text{OH}^-$  dissociation. Each B97-1 trajectory, which dissociated along the  $\text{CH}_3\text{I} + \text{OH}^-$  pathway, was recalculated using the CAM-B3LYP functional. The trajectory was restarted at the longest  $\text{CH}_3\text{I--OH}^-$  separation before dissociation where B97-1 was correct, i.e., an I–O distance of 3.0 Å, and then propagated with CAM-B3LYP. Each of these trajectories dissociated to  $\text{CH}_3\text{I} + \text{OH}^-$  as found for the B97-1 simulations and it was, thus, assumed that B97-1 gave the correct dissociation dynamics for the  $[\text{CH}_3\text{--I--OH}]^- \rightarrow \text{CH}_3\text{I} + \text{OH}^-$  pathway. CAM-B3LYP was also used to study the unimolecular dynamics of the  $[\text{CH}_3\text{--I--OH}]^-$  complex to compare with the B97-1 results. The CAM-B3LYP functional gives overall similar energies as compared with experimental values, and the CAM-B3LYP energies relative to  $\text{CH}_3\text{I} + \text{OH}^-$  are listed in Table 1, along with the B97-1 values.

The DFT calculations described above used a restricted closed-shell model, as used in our previous simulations for  $\text{S}_{\text{N}}2$  reactions.<sup>25–29</sup> However, for the current study,  $[\text{CH}_3\text{--I--OH}]^-$  can dissociate on its singlet PES to the  $\text{CH}_3 + \text{IOH}^-$  and  $\text{CH}_3\text{I}^- + \text{OH}$  doublet + doublet products; see Figure 1 (only the former was observed in the simulations). These dissociations were not described correctly by the restricted closed-shell DFT simulations, where the much higher energy  $\text{CH}_3^- + \text{IOH}$  singlet + singlet products were formed. In an attempt to get the proper branching to these doublet + doublet pathways, the dissociation of  $[\text{CH}_3\text{--I--OH}]^-$  was also simulated with open-shell B97-1 (only  $\text{CH}_3 + \text{IOH}^-$  was observed in these simulations and the much higher energy  $\text{CH}_3\text{I}^- + \text{OH}$  products were not formed) and open-shell CAM-B3LYP.

As for the restricted closed-shell B97-1 simulations, there were numerical problems with the open-shell B97-1 simulations.  $[\text{CH}_3\text{--I--OH}]^-$  dissociated to  $\text{CH}_3 + \text{IOH}^-$ , instead of  $\text{CH}_3^- + \text{IOH}$ , as found with closed-shell B97-1, but the dissociation was discontinuous with abrupt changes in the total energy and the negative charge on IOH; i.e., the latter “jumped” from  $\sim -0.6$  to  $-1.0$ . A second problem was the improper dissociation of  $[\text{CH}_3\text{--I--OH}]^-$  to  $\text{CH}_3 + \text{I}^{\delta-} + \text{OH}^{\delta-}$ , with a discontinuous jump in energy and fractional negative charges on I and OH. Initially, the dissociation involves OH departure with an  $\sim -0.8$  change on OH, as found for the closed-shell simulations, but then there were discontinuous jumps in the energy and the charge, with OH and I acquiring charges of  $-0.36$  and  $-0.64$ , respectively. In characterizing the open-shell simulation results, the discontinuous dissociations to the  $\text{CH}_3 + \text{IOH}^-$  products were counted as events for this pathway. However, the discontinuous dissociations to  $\text{CH}_3 + \text{I} + \text{OH}$ , forming I and OH with fractional negative charges, were counted as  $\text{CH}_3\text{I} + \text{OH}^-$  dissociation events, because the initial part of the dissociation to these products was numerically correct. Representative plots of distance, energy, and charge versus time are given in the Supporting Information for the

open-shell discontinuous  $[\text{CH}_3\text{--I--OH}]^-$  dissociations to the  $\text{CH}_3 + \text{IOH}^-$ ,  $\text{CH}_3\text{I} + \text{OH}^-$ , and  $\text{CH}_3 + \text{I}^{\delta-} + \text{OH}^{\delta-}$ .

**B. Direct Dynamics Simulations.** To probe the unimolecular dynamics of the  $[\text{CH}_3\text{--I--OH}]^-$  complex, it was excited by quantum microcanonical sampling at total energies of 50, 65, 75, and 100 kcal/mol, and then its decomposition was simulated by restricted B97-1/ECP/d direct dynamics. Quantum microcanonical sampling of the initial conditions for the trajectories has the potential of giving a microcanonical rate constant closer to the quantum microcanonical value than using classical microcanonical sampling.<sup>30,31</sup> Also, as discussed above, these B97-1 calculations were supplemented with CAM-B3LYP simulations. The above energies for B97-1 include the  $[\text{CH}_3\text{--I--OH}]^-$  ZPE of 28.8 kcal/mol, and the respective energies in excess of the ZPE are 21.2, 36.2, 46.2, and 71.2 kcal/mol. A randomly excited ensemble of  $[\text{CH}_3\text{--I--OH}]^-$  complexes was also simulated at a total energy of 100 kcal/mol using restricted CAM-B3LYP/ECP/d; i.e., the ZPE is 29.4 kcal/mol and the excess energy is 70.6 kcal/mol. In addition, open-shell simulations were performed at 100 kcal/mol excitation using both B97-1 and CAM-B3LYP.

The restricted closed-shell B97-1 trajectories were integrated for 10 ps at 50 and 75 kcal/mol, 12.5 ps at 65 kcal/mol, and 5.0 ps at 100 kcal/mol, using a sixth-order symplectic algorithm<sup>32,33</sup> with a 2.5 fs time step. Trajectories were also integrated with a velocity-Verlet algorithm<sup>34</sup> with a 0.25 fs time step to compare with the sixth-order symplectic algorithm trajectories. Both gave statistically the same dynamics, which were combined for the simulation results. These velocity-Verlet trajectories were integrated for 12.5 ps at 65 kcal/mol, 10 ps at 75 kcal/mol, and 5.0 ps at 100 kcal/mol. Average energy conservation for the six-order symplectic trajectories varied from 0.6% at 100 kcal/mol to 1.0% at 65 kcal/mol, with the conservation poorer for the latter as a result of the longer integration time. Energy conservation was poorer for the velocity-Verlet trajectories, with the average varying from 0.9% at 100 kcal/mol to 3.5% at 65 kcal/mol. The other 100 kcal/mol trajectories, with B97-1/open-shell, CAM-B3LYP/closed-shell, and CAM-B3LYP/open-shell, were integrated for 5.0 ps, using the velocity-Verlet algorithm with a 0.25 fs time step. Average energy conservation for the ensembles of B97-1/open-shell and CAM-B3LYP closed-shell and open-shell trajectories at 100 kcal/mol, was 3.9, 2.4, and 4.0%, respectively.

The total number of trajectories calculated depended on the theory, energy, and integration algorithm. For the six-order symplectic restricted B97-1 simulations, 161, 206, and 144 trajectories were calculated at 100, 75, and 65 kcal/mol, respectively. For these simulations with velocity-Verlet, the respective numbers are all 200. For the B97-1/closed-shell, CAM-B3LYP/open-shell, and CAM-B3LYP/open-shell simulations, at 100 kcal/mol, 100, 170, and 96 trajectories were calculated, respectively.

### III. SIMULATION RESULTS

**A. Dissociation Probability and Rate Constant.** As discussed above, the six-order symplectic and velocity Verlet B97-1/closed-shell trajectories gave statistically the same dynamics and, thus, the results of these integrations were combined to study  $[\text{CH}_3\text{--I--OH}]^-$  dissociation.

**1. B97-1 Closed-Shell and Open-Shell Trajectories.** For the 50 kcal/mol simulations,  $[\text{CH}_3\text{--I--OH}]^-$  has an energy of 21.2 kcal/mol in excess of its zero point energy, which is less than the lowest energy barrier of 24.1 kcal/mol with zero point

energies included. Thus, quantum mechanically, and neglecting tunneling for  $[\text{CH}_3\text{--I--OH}]^- \rightarrow \text{HO}^- \text{---HCH}_2\text{I}$  isomerization, no dissociations should occur at this energy. However, classical dynamics does not constrain and properly represent zero point energy effects, and dissociation is expected to occur for these classical simulations.<sup>35</sup> Nevertheless, for the 50 kcal/mol trajectories there were no  $[\text{CH}_3\text{--I--OH}]^-$  dissociations within 10 ps.

For the 65, 75, and 100 kcal/mol simulations dissociation of  $[\text{CH}_3\text{--I--OH}]^-$  occurred and the dissociation probability is presented by plotting, versus time, the logarithm of the relative number of  $[\text{CH}_3\text{--I--OH}]^-$  ions remaining at time  $t$ , i.e.,  $\ln[N(t)/N(0)]$ . As shown in Figure 3, the plots are approximately linear and the unimolecular rate constants obtained from the slopes are 0.019, 0.068, and 0.177  $\text{ps}^{-1}$  for 65, 75, and 100 kcal/mol, respectively.

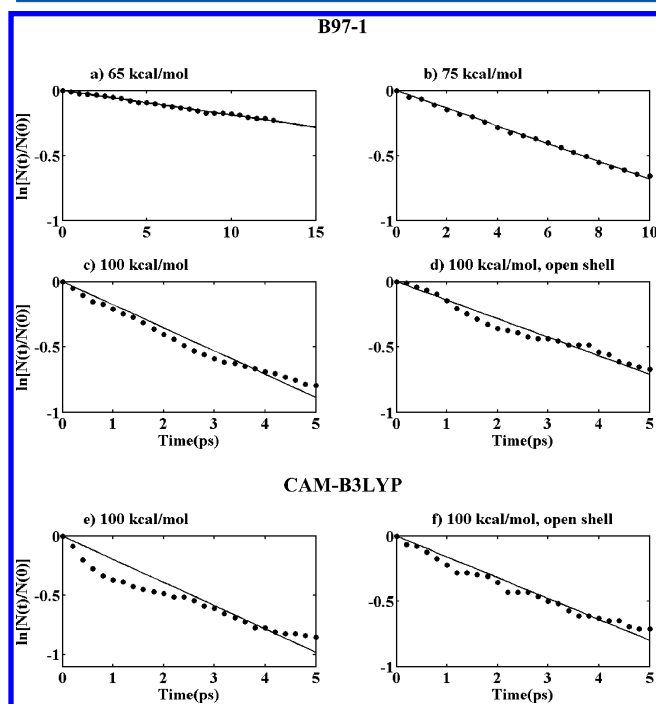


**Figure 3.** Plots of  $\ln[N(t)/N(0)]$  versus time for  $[\text{CH}_3\text{--I--OH}]^-$  dissociation, resulting from direct dynamics simulations of initial quantum microcanonical ensembles, at excitation energies of 65, 75, and 100 kcal/mol for the B97-1 and CAM-B3LYP functionals. The simulations are restricted, except for the two identified as open-shell.

The plot of  $\ln[N(t)/N(0)]$  versus  $t$  is shown in Figure 3d for the open-shell B97-1 trajectories at 100 kcal/mol. The unimolecular rate constant obtained from the approximately linear plot is 0.142  $\text{ps}^{-1}$  and similar to the value of 0.177  $\text{ps}^{-1}$  given above for the closed-shell simulations.

**2. CAM-B3LYP Closed-Shell and Open-Shell Trajectories.** Both closed-shell and open-shell CAM-B3LYP simulations were performed at 100 kcal/mol. Their plots of  $\ln[N(t)/N(0)]$  are shown in Figure 3e,f, respectively. Both plots are less linear than the B97-1 plots. Nevertheless, the rate constants obtained from the slopes of the plots are 0.196 and 0.160  $\text{ps}^{-1}$  for the closed-shell and open-shell simulation, respectively, which are similar to those for the B97-1 simulations.

**B. Product Branching Ratios.** The product branching ratios for the different simulations are given in Table 2. In the following the results for the B97-1 closed-shell and open-shell

simulations are first discussed, followed by a discussion of the CAM-B3LYP simulations.

**1. B97-1 Closed-Shell and Open-Shell Trajectories.** For the B97-1/closed-shell simulations at 65 kcal/mol, 21% of the trajectories dissociated at the termination point of 12.5 ps, and three product channels were observed. The ratio for forming the products  $\{\text{CH}_3\text{I} + \text{OH}^-\}:\{\text{CH}_2\text{I}^- + \text{H}_2\text{O}\}:\{\text{CH}_3\text{OH} + \text{I}^-\}$  is 0.87:0.09:0.04. At 75 kcal/mol, 36% of the  $[\text{CH}_3\text{--I--OH}]^-$  ions dissociated and the products  $\text{CH}_3\text{I} + \text{OH}^-$ ,  $\text{CH}_2\text{I}^- + \text{H}_2\text{O}$ ,  $\text{CH}_3\text{OH} + \text{I}^-$ , and  $\text{CH}_2 + \text{I}^- + \text{H}_2\text{O}$  were formed. The last is an additional channel as compared to the 65 kcal/mol simulations. The product ratio is  $\{\text{CH}_3\text{I} + \text{OH}^-\}:\{\text{CH}_2\text{I}^- + \text{H}_2\text{O}\}:\{\text{CH}_3\text{OH} + \text{I}^-\}:\{\text{CH}_2 + \text{I}^- + \text{H}_2\text{O}\} = 0.71:0.17:0.11:0.01$ . The dissociation probability is even higher for the closed-shell 100 kcal/mol simulation, where 56% of the  $[\text{CH}_3\text{--I--OH}]^-$  ions dissociated. As compared to the 75 kcal/mol simulation, there are two additional product channels, i.e.,  $\text{CH}_3^- + \text{IOH}$  and  $\text{CH}_2 + \text{I}^- (\text{H}_2\text{O})$ , where the latter is similar to the  $\text{CH}_2 + \text{I}^- + \text{H}_2\text{O}$  product channel except  $\text{I}^-$  is hydrated to form  $\text{I}^- (\text{H}_2\text{O})$ . The ratio for these products is  $\{\text{CH}_3\text{I} + \text{OH}^-\}:\{\text{CH}_2\text{I}^- + \text{H}_2\text{O}\}:\{\text{CH}_3\text{OH} + \text{I}^-\}:\{\text{CH}_3^- + \text{IOH}\}:\{\text{CH}_2 + \text{I}^- + \text{H}_2\text{O}\}:\{\text{CH}_2 + \text{I}^- (\text{H}_2\text{O})\} = 0.63:0.13:0.11:0.12:<0.01:<0.01$ . Because the yield of both the  $\text{CH}_2 + \text{I}^- + \text{H}_2\text{O}$  and  $\text{CH}_2 + \text{I}^- (\text{H}_2\text{O})$  product channels are smaller than 0.01, the sum of their yields are presented together in Table 2 as 0.01.

The closed-shell B97-1 trajectories do not properly dissociate to doublet radical products; e.g., these trajectories dissociate to the singlet products  $\text{CH}_3^- + \text{IOH}$ , instead of the lower energy  $\text{CH}_3 + \text{IOH}^-$  doublets (i.e., see energies in Figure 1). Such dissociations become important for the high energy 100 kcal/mol simulations, and open-shell B97-1 trajectories were calculated to compare with the above closed-shell B97-1 results. As discussed in section II.A, though open-shell B97-1 dissociated discontinuously to  $\text{CH}_3 + \text{IOH}^-$ , these dissociations were counted as reactive events.  $[\text{CH}_3\text{--I--OH}]^-$  also dissociated discontinuously to  $\text{CH}_3 + \text{I}^{\delta-} + \text{OH}^{\delta-}$ , with fractional charges on I and OH. However, the initial stage of this dissociation was numerically correct, with  $\text{I--OH}$  bond elongation, and in the analyses these dissociations were characterized as forming the  $\text{CH}_3\text{I} + \text{OH}^-$  products.

Though the closed-shell and open-shell B97-1 simulations give a similar rate constant for  $[\text{CH}_3\text{--I--OH}]^-$  dissociation (see above), as shown in Table 2 there are differences in their product branching ratios. As expected, open-shell B97-1 dissociates to  $\text{CH}_3 + \text{IOH}^-$ , instead of  $\text{CH}_3^- + \text{IOH}$ . The other major difference is the improper dissociation with the open-shell model to form the products  $\text{CH}_3 + \text{I}^{\delta-} + \text{OH}^{\delta-}$ , with fractional charges.

For the B97-1/open-shell simulation at 100 kcal/mol, 51% of trajectories dissociated, which is similar to the value of 56% for the closed-shell simulation. The ratio for the five product channels is  $\{\text{CH}_3\text{I} + \text{OH}^-\}:\{\text{CH}_2\text{I}^- + \text{H}_2\text{O}\}:\{\text{CH}_3\text{OH} + \text{I}^-\}:\{\text{CH}_3 + \text{IOH}^-\}:\{\text{CH}_4 + \text{IO}^-\} = 0.69:0.04:0.12:0.14:0.02$ . Neither the  $\text{CH}_2 + \text{I}^- + \text{H}_2\text{O}$  nor the  $\text{CH}_2 + \text{I}^- (\text{H}_2\text{O})$  product channels were formed for the open-shell simulation. A new product channel  $\text{CH}_4 + \text{IO}^-$  emerges, though with very low yield. As shown in Figure 1, the reaction energy for  $[\text{CH}_3\text{--I--OH}]^-$  dissociation to  $\text{CH}_4 + \text{IO}^-$  is 12.8 kcal/mol, which is the second lowest among the possible product channels. A high energy barrier may hinder the reactant  $[\text{CH}_3\text{--I--OH}]^-$  to follow this product channel, which may explain why  $\text{CH}_4 + \text{IO}^-$  is only formed at the high energy excitation of 100 kcal/mol. For the closed-shell simulation at 100 kcal/mol the product

Table 2. Product Branching Ratios for the Dissociation of  $[\text{CH}_3\text{-I-OH}]^-$  at Different Excitation Energies

	B97-1				CAM-B3LYP	
	closed shell		100 kcal/mol	open shell <sup>a</sup>	closed shell	open shell
	65 kcal/mol	75 kcal/mol		100 kcal/mol	100 kcal/mol	100 kcal/mol
dissociated	21%	36%	56%	51%	57%	52%
$\text{CH}_3\text{I} + \text{OH}^-$	$0.87 \pm 0.10$	$0.71 \pm 0.06$	$0.63 \pm 0.05$	$0.69 \pm 0.09$	$0.70 \pm 0.06$	$0.80 \pm 0.14$
$\text{CH}_2\text{I}^- + \text{H}_2\text{O}$	$0.09 \pm 0.03$	$0.17 \pm 0.03$	$0.13 \pm 0.02$	$0.04 \pm 0.03$	$0.19 \pm 0.04$	$0.12 \pm 0.07$
$\text{CH}_3\text{OH} + \text{I}^-$	$0.04 \pm 0.02$	$0.11 \pm 0.03$	$0.11 \pm 0.02$	$0.12 \pm 0.05$	$0.09 \pm 0.03$	$0.04 \pm 0.04$
$\text{CH}_3^- + \text{IOH}$			$0.12 \pm 0.02$			
$\text{CH}_3 + \text{IOH}^-$				$0.14 \pm 0.05$		
$\text{CH}_2 + \text{I}^- + \text{H}_2\text{O}^b$		$0.01 \pm 0.01$	$0.01 \pm 0.01$		$0.02 \pm 0.01$	$0.04 \pm 0.04$
$\text{CH}_4 + \text{IO}^-$				$0.02 \pm 0.02$		

<sup>a</sup>For the B97-1/open-shell 100 kcal/mol trajectories, the pathway  $\text{CH}_3 + \text{I}^{\delta-} + \text{OH}^{\delta-}$  is counted as the  $\text{CH}_3\text{I} + \text{OH}^-$  pathway, as discussed in sections II.A and III.B. <sup>b</sup>The  $\text{CH}_2 + \text{I}^-(\text{H}_2\text{O})$  trajectories are counted together with the  $\text{CH}_2 + \text{I}^- + \text{H}_2\text{O}$  trajectories for B97-1/closed-shell simulation at 100 kcal/mol.

Table 3. Distributions of Atomistic Mechanisms for the Three Product Pathways  $\text{CH}_3\text{I} + \text{OH}^-$ ,  $\text{CH}_2\text{I}^- + \text{H}_2\text{O}$ , and  $\text{CH}_3\text{OH} + \text{I}^-$ 

	B97-1				CAM-B3LYP	
	closed shell		100 kcal/mol	open shell	closed shell	open shell
	65 kcal/mol	75 kcal/mol		100 kcal/mol	100 kcal/mol	100 kcal/mol
$\text{CH}_3\text{I} + \text{OH}^-$						
direct	97%	97%	99%	95%	93%	95%
indirect	3%	3%	1%	5%	7%	5%
$\text{HO}^- \cdots \text{HCH}_2\text{I}$ complex	3%	3%	1%	5%	7%	5%
$\text{CH}_2\text{I}^- + \text{H}_2\text{O}$						
direct	43%	72%	88%	50%	72%	67%
indirect	57%	28%	12%	50%	28%	33%
$\text{CH}_2\text{I}^- \cdots \text{H}_2\text{O}$ complex	43%		4%			
$\text{HO}^- \cdots \text{HCH}_2\text{I}$ & $\text{CH}_2\text{I}^- \cdots \text{H}_2\text{O}$	14%					
$\text{HO}^- \cdots \text{HCH}_2\text{I}$		8%			11%	17%
proton exchange		4%				
PE & $\text{CH}_2\text{I}^- \cdots \text{H}_2\text{O}$		16%			11%	
$\text{CH}_3\text{OH} \cdots \text{I}^-$ complex			4%			
roundabout-like			4%	50%	6%	17%
$\text{CH}_3\text{OH} + \text{I}^-$						
direct	67%	76%	76%	67%	78%	50%
indirect	33%	24%	24%	33%	22%	50%
proton exchange	33%					
$\text{HO}^- \cdots \text{HCH}_2\text{I}$ & $\text{CH}_3\text{OH} \cdots \text{I}^-$		12%				
Barrier-recrossing		6%				
$\text{CH}_3\text{OH} \cdots \text{I}^-$ complex		6%	10%	17%		
$\text{HO}^- \cdots \text{HCH}_2\text{I}$ complex			5%		11%	
roundabout-like			10%	17%	11%	50%

ratio for the four dominant pathways is, as given above,  $\{\text{CH}_3\text{I} + \text{OH}^-\}:\{\text{CH}_2\text{I}^- + \text{H}_2\text{O}\}:\{\text{CH}_3\text{OH} + \text{I}^-\}:\{\text{CH}_3^- + \text{IOH}\} = 0.64:0.13:0.11:0.12$ . In contrast for the open-shell system, with  $\text{CH}_3 + \text{IOH}^-$  replacing  $\text{CH}_3^- + \text{IOH}$ , the ratio is  $0.70:0.04:0.12:0.14$ . The only significant difference in these ratios is for the  $\text{CH}_2\text{I}^- + \text{H}_2\text{O}$  product channel.

As the energy is lowered there are only three dominant B97-1/closed-shell product channels, which are  $\text{CH}_3\text{I} + \text{OH}^-$ ,  $\text{CH}_2\text{I}^- + \text{H}_2\text{O}$ , and  $\text{CH}_3\text{OH} + \text{I}^-$ . The primary dissociation channel is to the reactants  $\text{CH}_3\text{I} + \text{OH}^-$ . Its relative fraction, with respect to the three dominant channels, varies from 0.72–0.87 for the 65–100 kcal/mol energy range. The relative yield for  $\text{CH}_3\text{OH} + \text{I}^-$  decreased from 0.15 to 0.04 as the excitation energy decreased from 100 to 65 kcal/mol. With statistical uncertainties included, there is only a small decrease in the relative yield for  $\text{CH}_2\text{I}^- + \text{H}_2\text{O}$  with a decrease in energy. If

only the  $\text{CH}_3\text{I} + \text{OH}^-$ ,  $\text{CH}_2\text{I}^- + \text{H}_2\text{O}$ , and  $\text{CH}_3\text{OH} + \text{I}^-$  product channels are considered, the 100 kcal/mol B97-1/open-shell simulation gives their ratio as 0.81:0.05:0.14, with the relative yield for the  $\text{CH}_3\text{I} + \text{OH}^-$  product channel similar to the closed-shell result. The only difference is that the open-shell simulation has a higher yield for the  $\text{CH}_3\text{OH} + \text{I}^-$  product channel than for  $\text{CH}_2\text{I}^- + \text{H}_2\text{O}$ .

**2. CAM-B3LYP Closed-Shell and Open-Shell Trajectories.** For the CAM-B3LYP trajectories calculated at 100 kcal/mol, four product channels were found as shown in Table 2. Their ratio is  $\{\text{CH}_3\text{I} + \text{OH}^-\}:\{\text{CH}_2\text{I}^- + \text{H}_2\text{O}\}:\{\text{CH}_3\text{OH} + \text{I}^-\}:\{\text{CH}_2 + \text{I}^- + \text{H}_2\text{O}\} = 0.70:0.19:0.09:0.02$  for the closed-shell simulation, and the respective ratio for the open-shell simulation is 0.80:0.12:0.04:0.04. Interestingly, the  $\text{CH}_3^- + \text{IOH}$  products found with closed-shell B97-1, are not formed, and  $\text{CH}_3 + \text{IOH}^-$  is not formed for either the closed-shell or

open-shell CAM-B3LYP simulation. The B97-1/closed-shell ratio for  $\{\text{CH}_3\text{I} + \text{OH}^-\}:\{\text{CH}_2\text{I}^- + \text{H}_2\text{O}\}:\{\text{CH}_3\text{OH} + \text{I}^-\}$  is 0.73:0.15:0.12 and similar to the CAM-B3LYP/closed-shell result of 0.71:0.19:0.10. The statistical uncertainties in these ratios may be found from the branching fractions in Table 2. The ratio  $\{\text{CH}_3\text{I} + \text{OH}^-\}:\{\text{CH}_2\text{I}^- + \text{H}_2\text{O}\}:\{\text{CH}_3\text{OH} + \text{I}^-\}$  is 0.81:0.14:0.05 for the B97-1/open-shell simulation and 0.83:0.04:0.13 for CAM-B3LYP/open-shell simulation. The relative fraction of the  $\text{CH}_3\text{I} + \text{OH}^-$  product channel is similar for the two open-shell simulations, but the CAM-B3LYP/open-shell gave a much higher weight for the  $\text{CH}_3\text{OH} + \text{I}^-$  product channel.

**C. Atomistic Mechanisms for  $[\text{CH}_3\text{-I-OH}]^-$  Dissociation.** A study of the trajectories, for the chemical dynamics simulations, shows that  $[\text{CH}_3\text{-I-OH}]^-$  may dissociate directly to form the three dominant products  $\text{CH}_3\text{I} + \text{OH}^-$ ,  $\text{CH}_2\text{I}^- + \text{H}_2\text{O}$ , and  $\text{CH}_3\text{OH} + \text{I}^-$ . There are also indirect paths to form these products, as shown in Figure 2.  $[\text{CH}_3\text{-I-OH}]^-$  may isomerize to  $\text{CH}_3\text{OH}\cdots\text{I}^-$  or  $\text{HO}^-\cdots\text{HCH}_2\text{I}$ , with the latter possibly interconverting as  $\text{HO}^-\cdots\text{HCH}_2\text{I} \leftrightarrow \text{HOH}\cdots\text{CH}_2\text{I}^-$ . The isomerization may also be directly to the higher energy complex  $\text{CH}_2\text{I}^-\cdots\text{H}_2\text{O}$ ; see Figure 2. There is also a roundabout-like mechanism<sup>29</sup> in which the I $\cdots$ OH distance first extends, followed by  $\text{CH}_3$  rotating around the I atom for one or two full circles. The  $\text{OH}^-$  group then attacks the  $\text{CH}_3$  moiety directly forming either the  $\text{CH}_2\text{I}^- + \text{H}_2\text{O}$  or the  $\text{HO}^-\cdots\text{HCH}_2\text{I}$  complex. The latter may dissociate to  $\text{CH}_3\text{OH} + \text{I}^-$ . A barrier-recrossing mechanism<sup>3,36</sup> is also observed for the  $\text{CH}_3\text{OH} + \text{I}^-$  channel. Of interest is the relative importance of these mechanisms for the B97-1/closed-shell simulations with the 100, 75, and 65 kcal/mol excitation energies. The atomistic mechanisms were also studied at 100 kcal/mol with B97-1/open-shell, CAM-B3LYP/closed shell, and CAM-B3LYP/open-shell. The probabilities of the different atomistic mechanism are given in Table 3 and the mechanisms for the three most important pathways, i.e.,  $\text{CH}_3\text{I} + \text{OH}^-$ ,  $\text{CH}_2\text{I}^- + \text{H}_2\text{O}$ , and  $\text{CH}_3\text{OH} + \text{I}^-$ , are discussed in the following.

1.  **$\text{CH}_3\text{I} + \text{OH}^-$  Pathway.** The  $\text{CH}_3\text{I} + \text{OH}^-$  pathway is the most important for dissociation of  $[\text{CH}_3\text{-I-OH}]^-$  at all excitation energies, as discussed in section III.B and shown in Table 2. Among the  $\text{CH}_3\text{I} + \text{OH}^-$  trajectories, the majority were formed through a direct mechanism, which involved I–O bond stretching and  $\text{OH}^-$  departure from  $\text{CH}_3\text{I}$ . The percentages of the direct mechanism are around 95% for all the simulations; see Table 3. The remaining small percentage occurred indirectly via formation of the  $\text{HO}^-\cdots\text{HCH}_2\text{I}$  complex, where the O–I–C angle bent so that OH can interact with  $\text{CH}_3$  to form this complex for a short period of time. It should be noted that for the B97-1/open-shell simulations at 100 kcal/mol, although the  $\text{CH}_3 + \text{I}^{\delta-} + \text{OH}^{\delta-}$  trajectories were counted as the  $\text{CH}_3\text{I} + \text{OH}^-$  pathway (Table 2), the mechanism analyses here excludes these trajectories.

2.  **$\text{CH}_2\text{I}^- + \text{H}_2\text{O}$  Pathway.** The  $\text{CH}_2\text{I}^- + \text{H}_2\text{O}$  pathway is the second most important, with its percentage varying from 4% to 17% under different simulation conditions. Both direct and indirect mechanisms occurred for this product channel. For the B97-1/closed-shell simulations, the portion of indirect mechanisms increased from 12% to 57% as the excitation energy decreased from 100 to 65 kcal/mol.

The direct mechanism involved O–I–C bending, allowing the OH moiety to abstract one H atom upon interacting with  $\text{CH}_3$ . Then  $\text{H}_2\text{O}$  and  $\text{CH}_2\text{I}^-$  separated immediately. The formation and separation of the  $\text{CH}_2\text{I}^- + \text{H}_2\text{O}$  products was

too fast to allow formation of any possible complexes. This mechanism is very similar to the direct rebound mechanism in the previous study<sup>3,4</sup> of the  $\text{CH}_3\text{I} + \text{OH}^- \rightarrow \text{CH}_2\text{I}^- + \text{H}_2\text{O}$  reaction. The indirect mechanisms consist of the roundabout-like mechanism and formation of the complexes  $\text{HO}^-\cdots\text{HCH}_2\text{I}$ ,  $\text{CH}_3\text{OH}\cdots\text{I}^-$ ,  $\text{HOH}\cdots\text{CH}_2\text{I}^-$ , and  $\text{CH}_2\text{I}^-\cdots\text{H}_2\text{O}$  (Figure 2).

For the B97-1/closed-shell trajectories, at 65 kcal/mol, 43% of the dissociation is direct. Among the remaining 57% indirect mechanisms, 43% proceeded via formation of only the  $\text{CH}_2\text{I}^-\cdots\text{H}_2\text{O}$  complex, and 14% involved formation of both  $\text{HO}^-\cdots\text{HCH}_2\text{I}$  and  $\text{CH}_2\text{I}^-\cdots\text{H}_2\text{O}$ . Reaction at 75 kcal/mol is 72% direct and 28% indirect, where among the latter 8% occurred by forming the  $\text{HO}^-\cdots\text{HCH}_2\text{I}$  complex and 4% occurred through the proton-exchange mechanism  $\text{HO}^-\cdots\text{HCH}_2\text{I} \leftrightarrow \text{HOH}\cdots\text{CH}_2\text{I}^-$ , before dissociation to  $\text{CH}_2\text{I}^- + \text{H}_2\text{O}$ . The remaining 16% indirect trajectories not only experienced this proton exchange but also formed  $\text{CH}_2\text{I}^-\cdots\text{H}_2\text{O}$ , which then dissociated to  $\text{CH}_2\text{I}^- + \text{H}_2\text{O}$ . At 100 kcal/mol, the percentage of the direct mechanisms increased to 88%, with the remainder indirect. For the latter, 4% occurred by  $[\text{CH}_3\text{-I-OH}]^- \rightarrow \text{CH}_2\text{I}^-\cdots\text{H}_2\text{O}$  isomerization, and 4% occurred by  $[\text{CH}_3\text{-I-OH}]^- \rightarrow \text{CH}_3\text{OH}\cdots\text{I}^-$  isomerization, followed by dissociation to  $\text{CH}_2\text{I}^- + \text{H}_2\text{O}$ . The remaining 4% occurred by the roundabout-like mechanism, with  $\text{CH}_3$  rotating about the I atom and then reacting with  $\text{OH}^-$  to form  $\text{CH}_2\text{I}^- + \text{H}_2\text{O}$  during its second rotation.

The roundabout-like mechanism is a high-energy mechanism. It occurred for all the 100 kcal/mol simulations but did not occur at the lower excitation energies of 75 and 65 kcal/mol. The same trend is present for the  $\text{CH}_3\text{OH} + \text{I}^-$  pathway, discussed below.

For the other three sets of 100 kcal/mol simulations, half of the B97-1/open-shell trajectories are direct and half are indirect with the roundabout-like mechanism. Of the CAM-B3LYP/closed-shell trajectories 72% are direct, and among the remaining 28% indirect trajectories, 22% occurred via formation of either the  $\text{HO}^-\cdots\text{HCH}_2\text{I} \leftrightarrow \text{HOH}\cdots\text{CH}_2\text{I}^-$  or  $\text{CH}_2\text{I}^-\cdots\text{H}_2\text{O}$  complexes, and 6% by the roundabout-like mechanism. For the CAM-B3LYP/open-shell trajectories, 67% trajectories are direct, and half of the remaining indirect trajectories occurred through formation of the  $\text{HO}^-\cdots\text{HCH}_2\text{I}$  complex, with the other half following the roundabout-like mechanism.

3.  **$\text{CH}_3\text{OH} + \text{I}^-$  Pathway.** The mechanisms for dissociating  $[\text{CH}_3\text{-I-OH}]^-$  to  $\text{CH}_3\text{OH} + \text{I}^-$  are also classified as direct and indirect, as for the  $\text{CH}_3\text{I} + \text{OH}^-$  and  $\text{CH}_2\text{I}^- + \text{H}_2\text{O}$  pathways. The direct mechanism is very similar to the direct mechanism for the  $\text{CH}_2\text{I}^- + \text{H}_2\text{O}$  pathway, except  $\text{CH}_3\text{OH}$  is immediately formed as OH interacts with  $\text{CH}_3$ . If we use the same terminology as in the previous study<sup>2-4</sup> of the  $\text{CH}_3\text{I} + \text{OH}^- \rightarrow \text{CH}_3\text{OH} + \text{I}^-$  reaction, the direct mechanism here for  $[\text{CH}_3\text{-I-OH}]^- \rightarrow \text{CH}_3\text{OH} + \text{I}^-$  is called the direct rebound mechanism, and the indirect mechanisms may be classified as barrier-recrossing, roundabout-like, formation of the prereaction  $\text{HO}^-\cdots\text{HCH}_2\text{I}$  and/or postreaction  $\text{CH}_3\text{OH}\cdots\text{I}^-$  complexes, and proton-exchange  $\text{HO}^-\cdots\text{HCH}_2\text{I} \leftrightarrow \text{HOH}\cdots\text{CH}_2\text{I}^-$ . The majority of the trajectories proceeded by the direct mechanism for all the simulations.

For the B97-1/closed-shell trajectories, the percentage of the direct mechanisms is 67%, 76%, and 75% for the excitation energies of 65, 75, and 100 kcal/mol, respectively. For 65 kcal/mol, all of the 33% indirect reactions occurred via the proton-exchange mechanism  $\text{HO}^-\cdots\text{HCH}_2\text{I} \leftrightarrow \text{HOH}\cdots\text{CH}_2\text{I}^-$ . At 75 kcal/mol, 6% formed  $\text{CH}_3\text{OH} + \text{I}^-$  indirectly through barrier-

recrossing, and the remaining 18% indirect reaction occurred through formation of the  $\text{HO}^{\ominus}\text{---HCH}_2\text{I}$  prereaction and/or  $\text{CH}_3\text{OH---I}^{\ominus}$  postreaction complexes. At 100 kcal/mol, the roundabout-like mechanism occurred for 10%, and the  $\text{HO}^{\ominus}\text{---HCH}_2\text{I}$  prereaction and/or  $\text{CH}_3\text{OH---I}^{\ominus}$  postreaction complexes attribute for the remaining 15%.

Interestingly, besides the roundabout-like mechanism with  $\text{CH}_3$  rotating around the central I atom with the OH moiety fixed and far away from  $\text{CH}_3\text{I}$ , a new type of roundabout mechanism appeared. The C–I bond first extends, followed by  $\text{CH}_3$  rotation about IOH. Then  $\text{CH}_3$  reacts with OH to form the  $\text{CH}_3\text{OH}$  product. Although the  $\text{CH}_3$  group is able to rotate, making it possible to form the inversed-stereogeometric  $\text{CH}_3\text{OH}$ ,  $\text{CH}_3\text{OH}$  retained its stereogeometry. It is interesting to see both of these two types of roundabout-like mechanisms forming  $\text{CH}_3\text{OH} + \text{I}^{\ominus}$  for the high-energy 100 kcal/mol excitation of  $[\text{CH}_3\text{---I---OH}]^{\ominus}$ .

For the other 100 kcal/mol simulations, the respective percentages of the direct mechanism for B97-1/open-shell, CAM-B3LYP/closed-shell, and CAM-B3LYP/open-shell are 67%, 78%, and 50%. For the B97-1/open-shell simulations, half of the remaining indirect mechanisms are roundabout-like, and the other half occurred via the  $\text{CH}_3\text{OH---I}^{\ominus}$  postreaction complex. Likewise, half of the indirect CAM-B3LYP/closed-shell trajectories occurred via the roundabout-like mechanism, with the other half occurring via the  $\text{HO}^{\ominus}\text{---HCH}_2\text{I}$  prereaction complex. The only indirect mechanism for the CAM-B3LYP/open-shell simulation is the roundabout-like. It is noticeable that for the roundabout-like mechanism, one CAM-B3LYP/closed-shell trajectory occurred with  $\text{CH}_3$  rotating around the I atom two and one-half times, before finally reacting with OH to form  $\text{CH}_3\text{OH}$ .

#### IV. SUMMARY

In this work, the dissociation dynamics of the  $[\text{CH}_3\text{---I---OH}]^{\ominus}$  complex ion were studied by direct dynamics simulations utilizing both the B97-1 and CAM-B3LYP functionals with the ECP/d basis set, and with both restricted closed- and unrestricted open-shell theories. The majority of the simulations were performed with restricted B97-1 and it was found that with this method  $[\text{CH}_3\text{---I---OH}]^{\ominus}$  improperly dissociated to  $\text{CH}_3\text{I}$  and  $\text{OH}^{\ominus}$ , with fractional charges on each of the products. It is suspected that this problem may result from the DFT self-interaction error.<sup>21–23</sup> Restricted CAM-B3LYP simulations dissociated correctly to  $\text{CH}_3\text{I}$  and  $\text{OH}^{\ominus}$ . The B97-1 trajectories that improperly dissociated to  $\text{CH}_3\text{I} + \text{OH}^{\ominus}$  were repropagated with CAM-B3LYP and  $\text{CH}_3\text{I}$  and  $\text{OH}^{\ominus}$  were again formed, indicating that B97-1 dissociated to the correct products, but with incorrect fractional charges.

At high excitation energies  $[\text{CH}_3\text{---I---OH}]^{\ominus}$  may dissociate to the  $\text{CH}_3 + \text{IOH}^{\ominus}$  doublet products. However, instead of dissociating to these products, the restricted B97-1 simulations dissociated to the higher energy singlet products  $\text{CH}_3^{\ominus} + \text{IOH}$ . Unrestricted open-shell B97-1 and CAM-B3LYP simulations were performed to study the proper dissociation of  $[\text{CH}_3\text{---I---OH}]^{\ominus}$  to the  $\text{CH}_3 + \text{IOH}^{\ominus}$  products.

To study the effect of the excitation energy on the  $[\text{CH}_3\text{---I---OH}]^{\ominus}$  dissociation dynamics, B97-1/closed-shell simulations were performed at excitation energies of 50, 65, 75, and 100 kcal/mol. No  $[\text{CH}_3\text{---I---OH}]^{\ominus}$  complex ions dissociated at 50 kcal/mol for the 10 ps integrations. As the excitation increased from 65 to 100 kcal/mol, the dissociation percentage increased from 21% to 56%.  $[\text{CH}_3\text{---I---OH}]^{\ominus}$  dissociated exponentially

with respect to time and the dissociation rate constant obtained by a linear plot of  $\ln[N(t)/N(0)]$  versus  $t$ , where  $N(t)$  is the number of the  $[\text{CH}_3\text{---I---OH}]^{\ominus}$  complexes remaining at time  $t$ , is 0.019, 0.068, and  $0.177 \text{ ps}^{-1}$  for the excitation energies of 65, 75, and 100 kcal/mol, respectively. At 100 kcal/mol, unrestricted B97-1, restricted CAM-B3LYP, and unrestricted CAM-B3LYP give respective unimolecular rate constants of 0.142, 0.196, and  $0.160 \text{ ps}^{-1}$ , in good agreement with the restricted B97-1 value of  $0.177 \text{ ps}^{-1}$ .

For the 100 kcal/mol excitation simulations the restricted B97-1 product ratio for the six channels is  $\{\text{CH}_3\text{I} + \text{OH}^{\ominus}\}:\{\text{CH}_2\text{I}^{\ominus} + \text{H}_2\text{O}\}:\{\text{CH}_3\text{OH} + \text{I}^{\ominus}\}:\{\text{CH}_3^{\ominus} + \text{IOH}\}:\{\text{CH}_2 + \text{I}^{\ominus} + \text{H}_2\text{O}\}:\{\text{CH}_2 + \text{I}^{\ominus}(\text{H}_2\text{O})\} = 0.63:0.13:0.11:0.12:<0.01:<0.01$ , and the unrestricted B97-1 product ratio for the five channels is  $\{\text{CH}_3\text{I} + \text{OH}^{\ominus}\}:\{\text{CH}_2\text{I}^{\ominus} + \text{H}_2\text{O}\}:\{\text{CH}_3\text{OH} + \text{I}^{\ominus}\}:\{\text{CH}_3 + \text{IOH}^{\ominus}\}:\{\text{CH}_4 + \text{IO}^{\ominus}\} = 0.69:0.04:0.12:0.14:0.02$ . Only four product channels were found with CAM-B3LYP and for the restricted simulation the product ratio is  $\{\text{CH}_3\text{I} + \text{OH}^{\ominus}\}:\{\text{CH}_2\text{I}^{\ominus} + \text{H}_2\text{O}\}:\{\text{CH}_3\text{OH} + \text{I}^{\ominus}\}:\{\text{CH}_2 + \text{I}^{\ominus} + \text{H}_2\text{O}\} = 0.70:0.19:0.09:0.02$  and for the unrestricted simulation is  $0.80:0.12:0.04:0.04$ . With CAM-B3LYP the  $\text{CH}_3 + \text{IOH}^{\ominus}$  products are not formed for either the restricted or unrestricted simulation and the  $\text{CH}_3^{\ominus} + \text{IOH}$  products are not found with the restricted simulation. Each of the four simulations identify  $\text{CH}_3\text{I} + \text{OH}^{\ominus}$ ,  $\text{CH}_2\text{I}^{\ominus} + \text{H}_2\text{O}$ , and  $\text{CH}_3\text{OH} + \text{I}^{\ominus}$  as important products and the ratio  $\{\text{CH}_3\text{I} + \text{OH}^{\ominus}\}:\{\text{CH}_2\text{I}^{\ominus} + \text{H}_2\text{O}\}:\{\text{CH}_3\text{OH} + \text{I}^{\ominus}\}$  is  $0.72:0.15:0.13$  for the restricted B97-1 simulation,  $0.81:0.05:0.14$  for the unrestricted B97-1 simulation,  $0.71:0.19:0.10$  for the restricted CAM-B3LYP simulation, and  $0.83:0.13:0.04$  for the unrestricted CAM-B3LYP simulation. The  $\text{CH}_3\text{I} + \text{OH}^{\ominus}$  product channel is identified as most important for each of the four simulation methods, but they differ in the relative importance of the other two channels.

Restricted B97-1 simulations were used to study  $[\text{CH}_3\text{---I---OH}]^{\ominus}$  dissociation at lower energies where fewer dissociation channels were observed. At 65 kcal/mol three product channels were observed with the ratio  $\{\text{CH}_3\text{I} + \text{OH}^{\ominus}\}:\{\text{CH}_2\text{I}^{\ominus} + \text{H}_2\text{O}\}:\{\text{CH}_3\text{OH} + \text{I}^{\ominus}\}$  as  $0.87:0.09:0.04$ . At 75 kcal/mol there is one additional product and the product ratio is  $\{\text{CH}_3\text{I} + \text{OH}^{\ominus}\}:\{\text{CH}_2\text{I}^{\ominus} + \text{H}_2\text{O}\}:\{\text{CH}_3\text{OH} + \text{I}^{\ominus}\}:\{\text{CH}_2 + \text{I}^{\ominus} + \text{H}_2\text{O}\} = 0.71:0.17:0.11:0.01$ . At 75 kcal/mol the ratio of the three principal products is nearly the same as that at 100 kcal/mol. However, at 65 kcal/mol the yields of the  $\text{CH}_2\text{I}^{\ominus} + \text{H}_2\text{O}$  and  $\text{CH}_3\text{OH} + \text{I}^{\ominus}$  products may become less important.

Also studied were the atomic-level mechanisms for the three major product channels for  $[\text{CH}_3\text{---I---OH}]^{\ominus}$  dissociation, i.e.,  $\text{CH}_3\text{I} + \text{OH}^{\ominus}$ ,  $\text{CH}_2\text{I}^{\ominus} + \text{H}_2\text{O}$ , and  $\text{CH}_3\text{OH} + \text{I}^{\ominus}$ . Their mechanisms were classified as either direct or indirect. The majority of  $\text{CH}_3\text{I} + \text{OH}^{\ominus}$  were formed through a direct mechanism, with the remaining small percentage formed indirectly via the  $\text{HO}^{\ominus}\text{---HCH}_2\text{I}$  complex. For both the  $\text{CH}_2\text{I}^{\ominus} + \text{H}_2\text{O}$  and  $\text{CH}_3\text{OH} + \text{I}^{\ominus}$  product channels, the direct mechanism is overall more important than the indirect mechanisms. Various indirect mechanisms were identified, i.e., roundabout-like, barrier-recrossing, and formation of the complexes  $\text{HO}^{\ominus}\text{---HCH}_2\text{I}$ ,  $\text{CH}_3\text{OH---I}^{\ominus}$ ,  $\text{HOH---CH}_2\text{I}^{\ominus}$ , and  $\text{CH}_2\text{I}^{\ominus}\text{---H}_2\text{O}$ . Among these indirect mechanisms, the roundabout-like mechanism was only observed for the high-energy 100 kcal/mol simulations and was the most important indirect mechanism at this excitation energy. Mechanism comparisons between the B97-1 and CAM-B3LYP simulations at 100 kcal/mol showed that formation of the  $\text{CH}_3\text{OH---I}^{\ominus}$  complex is more favored for the B97-1 simulations, whereas formation of

the  $\text{HO}^- \cdots \text{HCH}_2\text{I}$  prereaction complex is more favored for the CAM-B3LYP simulations. The unrestricted simulations gave a higher percentage of indirect mechanisms than the restricted simulations.

The energy conservation for the restricted B97-1 simulations reported here was similar to that for our previous  $\text{OH}^- + \text{CH}_3\text{I}$  simulations,<sup>2–4</sup> but the unrestricted B97-1 and restricted and unrestricted CAM-B3LYP simulations were less accurate for large separation distances. In addition, there were discontinuities in the energy and Mulliken charge for the unrestricted B97-1 simulations. Several factors could be at play in these regions like the extent of the grids, basis functions and molecular orbital swapping due to the close vicinity of energy levels at large distances, but they do not affect the overall conclusions reported. Origin(s) of these numerical inaccuracies and instabilities will be investigated in detail in future work.

In conclusion, these simulations have given a detailed picture of the dynamics for  $[\text{CH}_3\text{-I-OH}]^-$  dissociation. They have also illustrated how different DFT methods give somewhat varying atomistic “pictures” of the dissociation dynamics. The simulation results presented here are very important for unraveling the role of the  $[\text{CH}_3\text{-I-OH}]^-$  complex ion in the dynamics of  $\text{OH}^-(\text{H}_2\text{O})_{n=1,2} + \text{CH}_3\text{I}$  reactions.

## ■ ASSOCIATED CONTENT

### Supporting Information

Plots of distance, Mulliken charge, and energy versus time for B97-1/open-shell trajectories for pathways  $\text{CH}_3\text{I} + \text{OH}^-$ ,  $\text{CH}_3 + \text{I}^{\delta-} + \text{OH}^{\delta-}$ , and  $\text{CH}_3 + \text{IOH}^-$  are provided. Direct dynamics simulation input files for VENUS/NWChem software package are given for B97-1 restricted closed-shell, B97-1 unrestricted open-shell, CAM-B3LYP restricted closed-shell, and CAM-B3LYP unrestricted open-shell trajectories. This material is available free of charge via the Internet at <http://pubs.acs.org>.

## ■ AUTHOR INFORMATION

### Corresponding Author

\*W. L. Hase. Phone: 806-834-3152. E-mail: [bill.hase@ttu.edu](mailto:bill.hase@ttu.edu).

### Notes

The authors declare no competing financial interest.

## ■ ACKNOWLEDGMENTS

The direct dynamics simulations reported here are based upon work supported by the Robert A. Welch Foundation under Grant No. D-0005. The simulations were performed on the Chemdynam cluster of the Hase research group. The authors acknowledge the Welch Summer Scholar Program which supported the summer research of Miranda McClellan. The authors also acknowledge important collaborations with the Roland Wester and Al Viggiano research groups regarding  $\text{S}_{\text{N}}2$  reaction dynamics. This work was done in part using EMSL, a national scientific user facility sponsored by the Department of Energy's Office of Biological and Environmental Research and located at Pacific Northwest National Laboratory, operated for the U.S. Department of Energy by Battelle under contract DE-AC05-76RL01830.

## ■ REFERENCES

- (1) Otto, R.; Brox, J.; Trippel, S.; Stei, M.; Best, T.; Wester, R. Single Solvent Molecules Can Affect the Dynamics of Substitution Reactions. *Nat. Chem.* **2012**, *4*, 534–438.
- (2) Otto, R.; Xie, J.; Brox, J.; Trippel, S.; Stei, M.; Siebert, M. R.; Hase, W. L.; Wester, R. Reaction Dynamics of Temperature-Variable

Anion Water Clusters Studied with Crossed Beams and by Direct Dynamics. *Faraday Discuss.* **2012**, *157*, 41–57.

(3) Xie, J.; Sun, R.; Siebert, M. R.; Otto, R.; Wester, R.; Hase, W. L. Direct Dynamics Simulations of the Product Channels and Atomistic Mechanisms for the  $\text{OH}^- + \text{CH}_3\text{I}$  Reaction. Comparison with Experiment. *J. Phys. Chem. A* **2013**, *117*, 7162–7178.

(4) Xie, J.; Kohale, S. C.; Hase, W. L.; Ard, S. G.; Melko, J. J.; Shuaman, N. S.; Viggiano, A. A. Temperature Dependence of the  $\text{OH}^- + \text{CH}_3\text{I}$  Reaction Kinetics. Experimental and Simulation Studies, and Atomic-Level Dynamics. *J. Phys. Chem. A* **2013**, *117*, 14019–14027.

(5) Xie, J.; Otto, R.; Mikosch, J.; Zhang, J.; Wester, R.; Hase, W. L. Identification of Atomic-Level Mechanisms for Gas-Phase  $\text{X}^- + \text{CH}_3\text{Y}$   $\text{S}_{\text{N}}2$  Reactions by Combined Experiments and Simulations. *Acc. Chem. Res.* **2014**, *47*, 2960–2969.

(6) Morris, R. A.; Viggiano, A. A. Kinetics of the Reactions of  $\text{F}^-$  with  $\text{CF}_3\text{Br}$  and  $\text{CF}_3\text{I}$  as a Function of Temperature, Kinetic Energy, Internal Temperature, and Pressure. *J. Phys. Chem.* **1994**, *98*, 3740–3746.

(7) Cyr, D. M.; Scarton, M. G.; Wiberg, K. B.; Johnson, M. A.; Nonse, S.; Hirokawa, J.; Tanaka, H.; Kondow, T.; Morris, R. A. Observation of the  $\text{XY}^-$  Abstraction Products in the Ion–Molecule Reactions  $\text{X}^- + \text{RY} \rightarrow \text{XY}^- + \text{R}$ : an Alternative to the  $\text{S}_{\text{N}}2$  Mechanism at Suprathermal Collision Energies. *J. Am. Chem. Soc.* **1995**, *117*, 1828–1832.

(8) Cyr, D. M.; Bisheal, G. A.; Scarton, M. G.; Johnson, M. A. Observation of Charge-Transfer Excited States in the  $\text{I}^- \cdot \text{CH}_3\text{I}$ ,  $\text{I}^- \cdot \text{CH}_3\text{Br}$ , and  $\text{I}^- \cdot \text{CH}_2\text{Br}_2$   $\text{S}_{\text{N}}2$  Reaction Intermediates Using Photo-fragmentation and Photoelectron Spectroscopies. *J. Chem. Phys.* **1992**, *97*, 5911–5914.

(9) Valiev, M.; Bylaska, E. J.; Govind, N.; Kowalski, K.; Straatsma, T. P.; van Dam, H. J. J.; Wang, D.; Nieplocha, J.; Apra, E.; Windus, T. L.; de Jong, W. A. NWChem: a Comprehensive and Scalable Open-Source Solution for Large Scale Molecular Simulations. *Comput. Phys. Commun.* **2010**, *181*, 1477–1489.

(10) Lourderaja, U.; Sun, R.; Kohale, S. C.; Barnes, G. L.; de Jong, W. A.; Windus, T. L.; Hase, W. L. The VENUS/NWChem Software Package. Tight Coupling between Chemical Dynamics Simulations and Electronic Structure Theory. *Comput. Phys. Commun.* **2014**, *185*, 1074–1080.

(11) Hase, W. L.; Duchovic, R. J.; Hu, X.; Komornicki, A.; Lim, K. F.; Lu, D. H.; Peshherbe, G. H.; Swamy, S. R.; Vande Linde, S. R.; Varandas, A.; et al. *Quantum Chemistry Program Exchange (QCPE) Bulletin* **1996**, *16*, 671.

(12) Hu, X.; Hase, W. L.; Pirraglia, T. Vectorization of the General Monte Carlo Classical Trajectory Program VENUS. *J. Comput. Chem.* **1991**, *12*, 1014–1024.

(13) Parr, R. G.; Yang, W. *Density Functional Theory of Atoms and Molecules*; Oxford University Press: New York, 1989.

(14) Becke, A. D. Density-Functional Thermochemistry. V. Systematic Optimization of Exchange-Correlation Functional. *J. Chem. Phys.* **1997**, *107*, 8554–8560.

(15) Hamprecht, F. A.; Cohen, A. J.; Tozer, D. J.; Handy, N. C. Development and Assessment of New Exchange-Correlation Functional. *J. Chem. Phys.* **1998**, *109*, 6264–6272.

(16) Zhang, J. X.; Hase, W. L. Electronic Structure Theory Study of the  $\text{F}^- + \text{CH}_3\text{I} \rightarrow \text{FCH}_3 + \text{I}^-$  Potential Energy Surface. *J. Phys. Chem. A* **2010**, *114*, 9635–9643.

(17) Dunning, T. H., Jr. Gaussian Basis Sets for Use in Correlated Molecular Calculations. I. The Atoms Boron Through Neon and Hydrogen. *J. Chem. Phys.* **1989**, *90*, 1007–1023.

(18) Woon, D. E.; Dunning, T. H., Jr. Gaussian Basis Sets for Use in Correlated Molecular Calculations. III. The Atoms Aluminum through Argon. *J. Chem. Phys.* **1993**, *98*, 1358–1371.

(19) Wadt, W. R.; Hay, P. J. *Ab initio* Effective Core Potentials for Molecular Calculations. Potentials for Main Group Elements Na to Bi. *J. Chem. Phys.* **1985**, *82*, 284–298.

(20) Hu, W. P.; Truhlar, D. G. Structural Distortion of  $\text{CH}_3\text{I}$  in an Ion-Dipole Precursor Complex. *J. Phys. Chem.* **1994**, *98*, 1049–1052.

- (21) Perdew, J. P.; Zunger, A. Self-interaction Correction to Density-Functional Approximations for Many-Electron Systems. *Phys. Rev. B* **1981**, *23*, 5048–5079.
- (22) Zhang, Y.; Yang, W. A Challenge for Density Functionals: Self-Interaction Error Increases for Systems with A Noninteger Number of Electrons. *J. Chem. Phys.* **1998**, *109*, 2604–2608.
- (23) Mori-Sánchez, P.; Cohen, A. J.; Yang, W. Many-Electron Self-Interaction Error in Approximate Density Functionals. *J. Chem. Phys.* **2006**, *125*, 201102.
- (24) Yanai, T.; Tew, D. P.; Handy, N. C. A New Hybrid Exchange–Correlation Functional Using the Coulomb-Attenuating Method (CAM-B3LYP). *Chem. Phys. Lett.* **2004**, *393*, 51–57.
- (25) Zhang, J.; Mikosch, J.; Trippel, S.; Otto, R.; Weidemüller, M.; Wester, R.; Hase, W. L.  $F^- + CH_3I \rightarrow FCH_3 + I^-$  Reaction Dynamics. Nontraditional Atomistic Mechanisms and Formation of a Hydrogen-Bonded Complex. *J. Phys. Chem. Lett.* **2010**, *1*, 2747–2752.
- (26) Mikosch, J.; Zhang, J.; Trippel, S.; Eichhorn, C.; Otto, R.; Sun, R.; de Jong, W. A.; Weidemüller, M.; Hase, W. L.; Wester, R. Indirect Dynamics in a Highly Exoergic Substitution Reaction. *J. Am. Chem. Soc.* **2013**, *135*, 4250–4259.
- (27) Zhang, J.; Lourderaj, U.; Sun, R.; Mikosch, J.; Wester, R.; Hase, W. L. Simulation Studies of the  $Cl^- + CH_3I$   $S_N2$  Nucleophilic Substitution Reaction: Comparison with Ion Imaging Experiments. *J. Chem. Phys.* **2013**, *138*, 114309.
- (28) Sun, R.; Davda, C.; Zhang, J.; Hase, W. L. Comparison of Direct Dynamics Simulations with Different Electronic Structure Methods.  $F^- + CH_3I$  with MP2 and DFT/B97-1. *Phys. Chem. Chem. Phys.* **2015**, *17*, 2589–2597.
- (29) Mikosch, J.; Trippel, S.; Eichhorn, C.; Otto, R.; Lourderaj, U.; Zhang, J. X.; Hase, W. L.; Weidemüller, M.; Wester, R. Imaging Nucleophilic Substitution Dynamics. *Science* **2008**, *319*, 183–186.
- (30) Paranjothy, M.; Hase, W. L. Comparisons of Classical Chemical Dynamics Simulations of the Unimolecular Decomposition of Classical and Quantum Microcanonical Ensembles. *J. Chem. Phys.* **2012**, *136*, 184110.
- (31) Park, K.; Engelkemier, J.; Persico, M.; Manikandan, P.; Hase, W. L. Algorithms for Sampling a Quantum Microcanonical Ensemble of Harmonic Oscillators at Potential Minima and Conical Intersections. *J. Phys. Chem. A* **2011**, *115*, 6603–6609.
- (32) Schlier, C.; Seiter. Symplectic Integration of Classical Trajectories: A Case Study. *A. J. Phys. Chem. A* **1998**, *102*, 9399–9404.
- (33) Schlier, C.; Seiter, A. High-Order Symplectic Integration: An Assessment. *Comput. Phys. Commun.* **2000**, *130*, 176–189.
- (34) Verlet, L. Computer “Experiments” on Classical Fluids. I. Thermodynamical Properties of Lennard–Jones Molecules. *Phys. Rev.* **1967**, *159*, 98–103.
- (35) Hase, W. L.; Buckowski, D. G. Dynamics of Ethyl Radical Decomposition. II. Applicability of Classical Mechanics to Large-Molecule Unimolecular Reaction Dynamics. *J. Comput. Chem.* **1982**, *3*, 335–343.
- (36) Vande Linde, S. R.; Hase, W. L. Non-RRKM Kinetics in Gas-Phase  $S_N2$  Nucleophilic Substitution. *J. Phys. Chem.* **1990**, *94*, 6148–6150.